atmosphere

MDPI

Article

Regional Transport Increases Ammonia Concentration in Beijing, China

Qingmei Wang [1], Yucong Miao [2,*] and Ligang Wang [1,*]

[1] Institute of Agricultural Resources and Regional Planning, Chinese Academy of Agricultural Sciences, Beijing 100081, China; wangqm1015@163.com
[2] Chinese Academy of Meteorological Sciences, Beijing 100081, China
* Correspondence: miaoyucong@yeah.net (Y.M.); wangligang@caas.cn (L.W.)

Received: 2 May 2020; Accepted: 26 May 2020; Published: 28 May 2020

Abstract: To elucidate the critical factors influencing the ammonia (NH_3) concentration in Beijing, this study combined observational analyses, backward trajectory calculations, and meteorology–chemistry coupled simulations to investigate the variations in the NH_3 concentration from 11 May to 24 June, 2015. A significant positive correlation was found between the NH_3 and $PM_{2.5}$ concentrations in Beijing. By examining the relationships between meteorological parameters and the NH_3 concentration, both near-surface temperature and relative humidity showed positive correlations with the NH_3 concentration. The higher NH_3 concentrations were usually associated with the warming of the upper atmosphere. Distinct wind directions were noted during the days of the top and bottom 33.3% NH_3 concentrations. The top 33.3% concentrations were primarily related to southwesterly winds, while the bottom ones were associated with westerly and northerly winds. Since there are strong NH_3 emissions in the southern plains adjacent to Beijing, the regional transport induced by the southerly prevailing winds would increase the NH_3 concentration in Beijing significantly. From 23 to 25 May, more than one third of NH_3 in Beijing was contributed by the southerly transport processes. Thus, joint efforts to reduce NH_3 emissions in the whole Beijing–Tianjin–Hebei region are necessary to regulate the NH_3 concentration in Beijing.

Keywords: regional transport; WRF-Chem; backward trajectory analysis; thermal stratification

1. Introduction

Being the most abundant basic/alkaline gas species in the atmosphere, ammonia (NH_3) plays an important role in determining the overall acidity of precipitation, cloud water, and airborne particulate matter [1,2]. The largest source of NH_3 emission is agriculture, including animal husbandry and NH_3-based fertilizer applications [2]. Sutton et al. estimated that 57% of global atmospheric NH_3 was emitted from crop and livestock production in 2008 [1]. Once emitted into the atmosphere, NH_3 undergoes complex atmospheric processes such as transformation due to reactions, transport associated with winds, and wet and dry deposition [3].

During the past decades, the rapid development of economy and urbanization in China have led to poor air quality and high $PM_{2.5}$ (particle matter with an aerodynamic diameter less than 2.5 μm) loading in most cities, particularly in the densely populated Beijing–Tianjin–Hebei region [4,5]. Among the aerosol precursors, several studies have pointed out the importance of NH_3 [6–9], which acts as a limiting species in the formation of secondary inorganic aerosols (SIA). In the atmosphere, NH_3 can neutralize ambient acidic species, such as sulfuric acid (H_2SO_4) and nitric acid (HNO_3), to form ammonium salts, which are the dominant inorganic compounds in the ambient $PM_{2.5}$ [2,10]. These reaction pathways link NH_3 to aerosol pollution and its subsequent impacts on human health and climate change [11,12]. It was found that the mass of secondary sulfate, nitrate, and ammonium

accounted for 25–60% of the total $PM_{2.5}$ concentration [13,14]. The total NH_3 emission in China in 2015 was estimated to be 15.6 ± 0.9 Tg N yr^{-1} [6]. Such a high emission rate makes NH_3 become one of the critical species related to the air pollution issues in China. Long-term measurements of NH_3 in Shanghai of China demonstrated the important role of the gas-to-particle conversion of NH_3 on $PM_{2.5}$ formation [15], and the ammonium accounted for about 10% of the $PM_{2.5}$ concentration measured in Shanghai [15]. The gas-to-particle conversion of NH_3 was also observed to lead to a significant increase of ammonium during haze events in Beijing [16,17]. The chemical composition analysis of $PM_{2.5}$ in Beijing indicated that the ammonium accounted for 11% of the total defined $PM_{2.5}$ components during the heavily polluted days [16,17]. In addition, the atmospheric deposition of NH_3 into terrestrial and aquatic ecosystems can cause adverse environmental effects, such as soil acidification, eutrophication of water bodies, and even plant biodiversity reduction [2,18–21]. Although the environmental impacts of NH_3 in China have been recognized [10,13], until now, the NH_3 emissions have not been regulated by the Chinese government; by contrast, stringent measures have been taking to control the emissions of sulfur dioxide (SO_2) and nitrogen oxide (NO_X) [22]. Since the balance between SO_2, NO_X, and NH_3 emissions will define cation- or anion-limited regimes of inorganic aerosol formation [23,24], it is suggested to consider the regulation of NH_3 emissions as a possible measure to mitigate the heavy aerosol pollution in some regions of China [24].

The atmospheric NH_3 concentration in Beijing is not only contributed by local emission sources (e.g., traffic exhaust, husbandry), but can also be influenced by adjacent agricultural emissions from surrounding croplands (Figure 1) under certain synoptic conditions [25,26]. Based on one-year observations of the vertical distribution of NH_3 at the 325-m meteorological tower in Beijing, Zhang et al. found that air masses from the agricultural regions contributed most to the high NH_3 concentration measured [27]. At a rural site in the Beijing–Tianjin–Hebei region, Meng et al. also observed that the increased NH_3 concentration was associated with specific wind directions, and suggested that the transport of NH_3 emitted from agricultural regions was critical to the air quality in the downstream regions [25]. Although the regional transport of NH_3 in the Beijing–Tianjin–Hebei region has been documented, the potential source region to Beijing and to what extent the regional transport influences the NH_3 concentration in Beijing are not yet clearly understood.

To identify the potential source regions, and quantitatively evaluate the impacts of regional transport on the NH_3 concentration in Beijing, this study combines observational analyses, backward trajectory calculations, and meteorology–chemistry coupled simulations to systematically investigate the transport processes of NH_3 in the Beijing–Tianjin–Hebei region. The rest of this paper is organized as follows. In Section 2, the methods and data are described. In Section 3, the impacts of regional transport on NH_3 concentration in Beijing are analyzed. Finally, the main findings are summarized in Section 4.

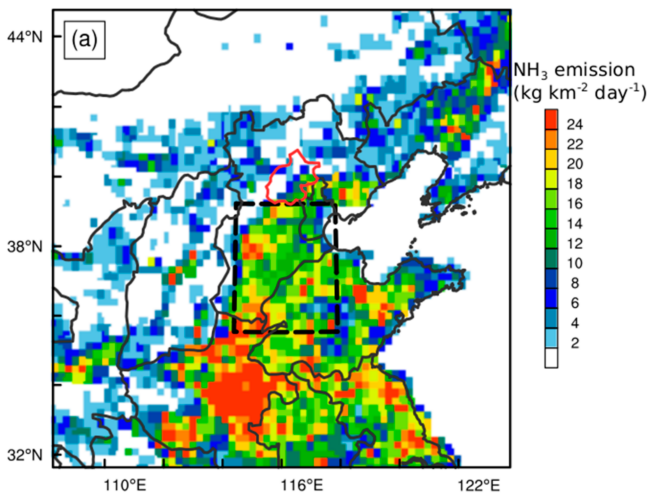

Figure 1. *Cont.*

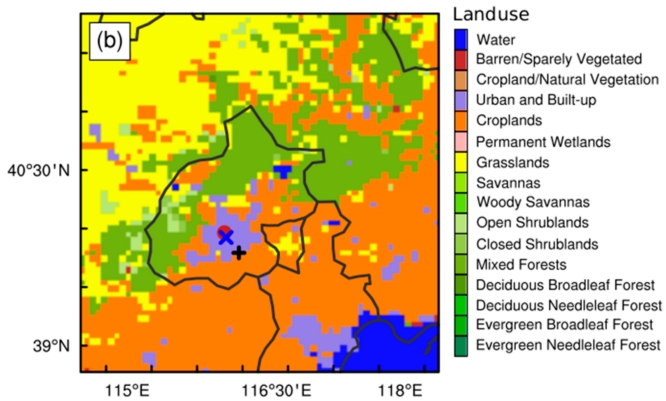

Figure 1. Maps of (**a**) Weather Research and Forecasting model coupled with chemistry (WRF-Chem) simulation domain and anthropogenic NH_3 emissions in May, 2016, and (**b**) the land use types in Beijing and its adjacent regions. The location of Beijing is denoted by the red lines in Figure 1a, and the locations of the NH_3 monitoring site, $PM_{2.5}$ monitoring site, and meteorological site in Beijing are marked by the blue cross, red dot, and black plus in Figure 1b, respectively. The dashed rectangle in Figure 1a indicates the regions using the emission zero-out method in the WRF-Chem simulation.

2. Methods and Data

To understand the variations in NH_3 concentration in Beijing, hourly NH_3 concentration from 11 May to 24 June in 2015 was measured in the Beijing Municipal Environmental Monitoring Center (116.32° E, 39.93° N; marked by the blue cross in Figure 1b) using a differential optical absorption spectroscope (DOAS, Anhui Landun Photoelectron Co. Ltd., Tongling, Anhui, China). The DOAS, an open-path monitoring technique, is based on the wavelength dependent absorption of light over a specified light path [28]. It is often utilized in the UV and visible parts of the electromagnetic spectrum. The absorption lines and bands of gas molecules in this part of the spectrum are caused by electronic transitions and their shapes only weakly depend on temperature and pressure [28]. Regarding NH_3, it has a strong absorption band with narrowband features in the UV part from 170 to 220 nm [29], and the DOAS system can monitor its concentration with a high accuracy of 0.04 μg m^{-3} for a total light path of 100 m [30]. In this study, both the transmitter and retro-reflector were placed 20 m high above the ground [30]. The detailed information of the NH_3 measurement in the Beijing Municipal Environmental Monitoring Center can be found in the previous study of Cheng et al. [30]. The $PM_{2.5}$ concentration in Beijing (116.31° E, 39.97° N; marked by the red dot in Figure 1b) was also collected from the China National Environmental Monitoring Center. Besides, both the ground-level and upper-air meteorological observations in the southern Beijing (116.47° E, 39.80° N, marked by the black plus in Figure 1b) were obtained. The ground-level meteorological parameters were recorded hourly, while the sounding balloons were launched twice a day at 08:00 and 20:00 local time (LT = UTC + 8h). In total, 45-day measurements in Beijing were collected, including the near-surface NH_3 and $PM_{2.5}$ concentrations, 2-m temperature (T), 2-m relative humidity (RH), precipitation and the vertical profiles of the potential temperature (PT) and horizontal winds.

Through analyzing these observational data, the relationships between the meteorological conditions and NH_3 concentration in Beijing were elucidated, and then a typical pollution episode (23–25 May) associated with southerly prevailing winds was selected and simulated using the Weather Research and Forecasting model coupled with chemistry (WRF-Chem) [31]. The simulation domain was centered in the Beijing–Tianjin–Hebei region with a horizontal resolution of 11 km, covering an area of 106–126° E in longitude and 31–45° N in latitude (Figure 1a). In the vertical dimension, 33 vertical layers were set from the surface to the 10-hPa level, of which 15 layers were set below 2 km above ground-level (AGL). The physics parameterization schemes used in the WRF-Chem simulation included the Noah land surface scheme [32], Yonsei University (YSU) boundary layer scheme [33], rapid radiative transfer model for general circulation (RRTMG) long-/short-wave radiation scheme [34],

Betts–Miller–Janjic cumulus scheme [35], and WRF single-moment-5-class microphysics scheme [36]. Regarding the chemical processes, the RADM2-MADE/SORGAM mechanism [37–39] was used with the Multi-resolution Emission Inventory for China (MEIC), and the dry and wet deposition schemes were turned on. The MEIC is the most updated and widely used emission data available for the studied region, which is developed and provided by Tsinghua University [40]. The WRF-Chem simulation was initialized at 20:00 LT on 21 May, and ran for 100 h until 00:00 LT on 26 May. The first 28 h were considered as a spin-up period. The initial and boundary conditions of the meteorological variables were configured using the 5th generation of atmospheric reanalysis produced by European Centre for Medium-Range Weather Forecasts (ERA5), and the initial and boundary conditions of the chemical variables were derived from the output of a global chemical transport model [41]. In the rest, the simulation using these configurations is referred to as the baseline (BASE) run.

To identify the potential source regions, for each day of the selected episode, 24-h air mass backward trajectories were calculated using the hybrid single particle Lagrangian integrated trajectory model (HYSPLIT, developed by the Air Resource Laboratory of the United States National Oceanic and Atmospheric Administration, College Park, Maryland, US). The model has been widely applied to identify the air mass origins and pathways that reach the receptor sites [42]. The ending point was set using the location of the NH_3 monitoring site (116.32° E, 39.93° N) with a height of 100 m AGL, and the ending time was 18:00 LT of each day. According to those backward trajectories, a sensitivity numerical experiment was designed using the emission zero-out method [26,43], in which all the anthropogenic emissions in the possible source region were set to zero. Except for the emission configuration, the other settings of the sensitivity experiment used were the same settings of the BASE run. The sensitivity experiment is referred to as the EXP run hereafter. Thereby, the contributions of regional transport to the NH_3 concentration in Beijing can be roughly estimated as the simulation differences between the BASE and EXP runs. In the rest of this paper, the simulation results presented and discussed are derived from the BASE run unless otherwise noted.

Besides, to examine the effects of emission control measures on the aerosol pollution in Beijing, two more sensitivity simulations (i.e., SIM-1 and SIM-2) were conducted using the same settings of the BASE run except for the emissions. In SIM-1, the emissions of SO_2 and NO_X in the whole simulation domain were reduced by 50%. In SIM-2, the changes in SO_2 and NO_X emissions were the same as those in SIM-1, and the emissions of NH_3 were also reduced by 50%.

3. Results and Discussion

3.1. Relationships between NH_3 Concentration and Meteorological Parameters

The time series of the daily NH_3 concentration from 11 May to 24 June in Beijing is shown in Figure 2a. The peak daily NH_3 concentration was 34.6 μg m^{-3} on 17 May, and the minimum concentration was 2.0 μg m^{-3} on 19 May. During the studied period, there were in total 12 rainy days in Beijing (Figure 2c). To isolate the complex impacts of precipitation on air pollution [44], only the measurements of the rest 33 days under dry conditions were further analyzed in this study. After excluding the rainy days, the relationships between the NH_3 concentrations and near-surface meteorological parameters in Beijing were examined (Figure 2b,c). It was found that the daily NH_3 concentration was positively correlated with the near-surface T and RH, with correlation coefficients of 0.49 and 0.65, respectively. The link between the vertical thermal stratification and ground-level NH_3 concentration in Beijing was also investigated based on the sounding data at 20:00 LT. The higher NH_3 concentrations in Beijing were usually associated with the warming of the upper atmosphere (Figure 2d), such as the episodes that occurred around 25 May and 1 June. As a result, a significant positive correlation was found between the 1500-m PT and NH_3 concentration in Beijing (R = 0.72). Such a relationship can be explained by the development of the boundary layer and its impact on the pollutants' vertical dispersion. The warming aloft can increase the thermal stability, which would suppress the development of the boundary layer to some extent, as well as the vertical dispersion

and dilution of pollutants [5,45,46]. Besides, we compared the NH_3 concentrations with the $PM_{2.5}$ concentrations, and a significant positive correlation (R = 0.75) was found (Figure 2a). It can be explained by the day-to-day variations in the meteorological conditions that caused the simultaneous increase or drop in the NH_3 and $PM_{2.5}$ concentrations. On the other hand, NH_3 is also intricately linked to the secondary formation of aerosols [22–24], which is relevant to the acidity (pH), liquid water content and HNO_3 level [47,48].

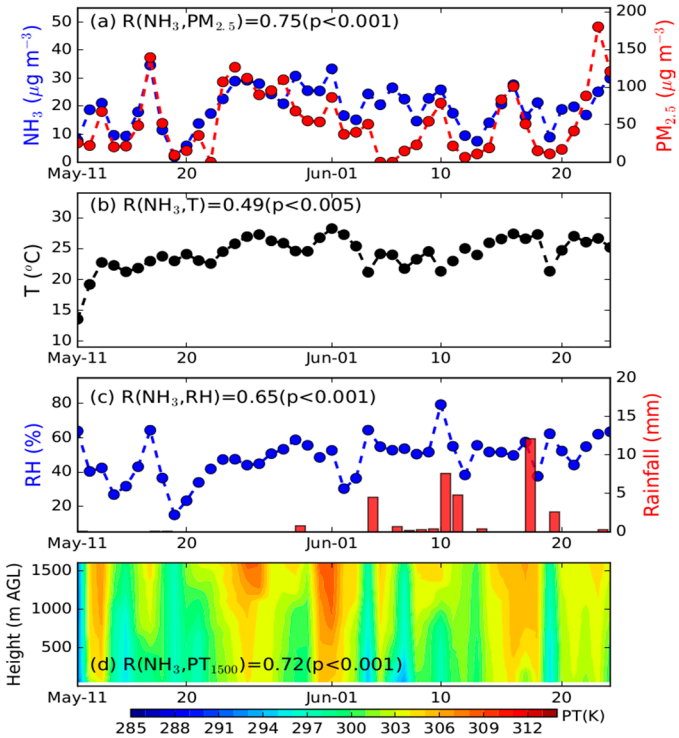

Figure 2. Daily variations in (**a**) NH_3 and $PM_{2.5}$ concentrations, (**b**) 2-m temperature (T), (**c**) 2-m relative humidity (RH), and rainfall, (**d**) potential temperature vertical profile in Beijing from 11 May to 24 June, 2015. There were in total 12 rainy days during the studied period, and the correlation coefficients (R) between the NH_3 concentration and different variables in Beijing under dry conditions are given for each panel, including the $PM_{2.5}$ concentration, T, RH and 1500-m PT.

To further understand the factors leading to the increased NH_3 concentrations in Beijing, Figure 3 and Table 1 compare the different characteristics associated with the top and bottom 33.3% daily NH_3 concentrations under dry conditions. The top 33.3% NH_3 concentrations in Beijing were within 22.4–34.6 μg m^{-3}, significantly higher than the bottom 33.3% concentrations (2.0–16.6 μg m^{-3}). When the top 33.3% concentrations happened, the average 2-m T and 2-m RH in Beijing were 26.0 °C and 52%, respectively, significantly warmer and moister than those associated with the bottom 33.3% concentrations (i.e., 23.1 °C and 35%). At the upper levels, the thermal difference between the days associated with the top and bottom 33.3% concentrations was larger; the average values of the 1500-m PT were 305.6 K and 300.7 K, respectively. In short, the warmer and moister conditions and appearance of strong thermal inversion aloft in Beijing favor the accumulation of NH_3.

In addition, distinct wind directions could be found based on the wind measurements at 800-m AGL (close to the 925-hPa level). The top 33.3% NH_3 concentrations in Beijing were primarily in relation to the southwesterly winds (181–225°), while the bottom 33.3% NH_3 concentrations were corresponding to the westerly and northerly winds (226–360°). Since there are strong NH_3 emissions in the southern plains adjacent to Beijing (Figure 1a), it is hypothesized that the regional transport of NH_3 induced by the southerly prevailing winds is critical to the increased NH_3 concentration in Beijing. To quantitatively evaluate the impact of regional transport, the episode from 23 to 25 May associated

with the southwesterly prevailing winds was simulated using WRF-Chem and further analyzed in the Section 3.2.

Table 1. NH_3 concentrations, 2-m T, 2-m RH, 1500-m PT and 800-m wind direction (WD) in Beijing during the dry conditions from 11 May to 24 June, 2015. Except for that the PT and WD are presented according to the soundings at 20:00 LT, the other variables are derived from the daily mean values.

	Date (Month-Day)	NH_3 (μg m^{-3})	T (°C)	RH (%)	PT_{1500} (K)	WD_{800} (°)
Days with Top 33.3% Daily NH_3 Concentrations	05-17	34.6	22.9	64	304.6	217
	05-23	22.6	24.5	47	303.8	208
	05-24	28.9	25.8	48	305.4	220
	05-25	29.2	26.9	44	307.9	215
	05-26	28.0	27.3	45	307.9	217
	05-27	24.4	26.2	51	303.5	231
	05-30	25.5	24.5	56	302.0	183
	05-31	25.4	26.7	49	308.3	214
	06-01	33.3	28.2	53	308.9	209
	06-16	27.6	27.4	50	305.4	267
	06-24	29.9	25.2	64	303.3	218
Days with Bottom 33.3% Daily NH_3 Concentrations	05-11	7.8	13.5	64	291.2	337
	05-14	9.6	22.3	27	301.3	205
	05-15	9.3	21.2	32	298.8	235
	05-18	11.5	23.7	37	300.4	345
	05-19	2.0	23.0	15	297.1	348
	05-20	5.8	24.1	23	301.4	242
	05-21	13.8	23.0	34	302.7	229
	06-02	16.6	27.2	30	305.0	353
	06-03	15.1	25.4	36	304.6	234
	06-12	9.5	25.0	38	301.7	302
	06-14	14.1	25.9	52	303.9	184

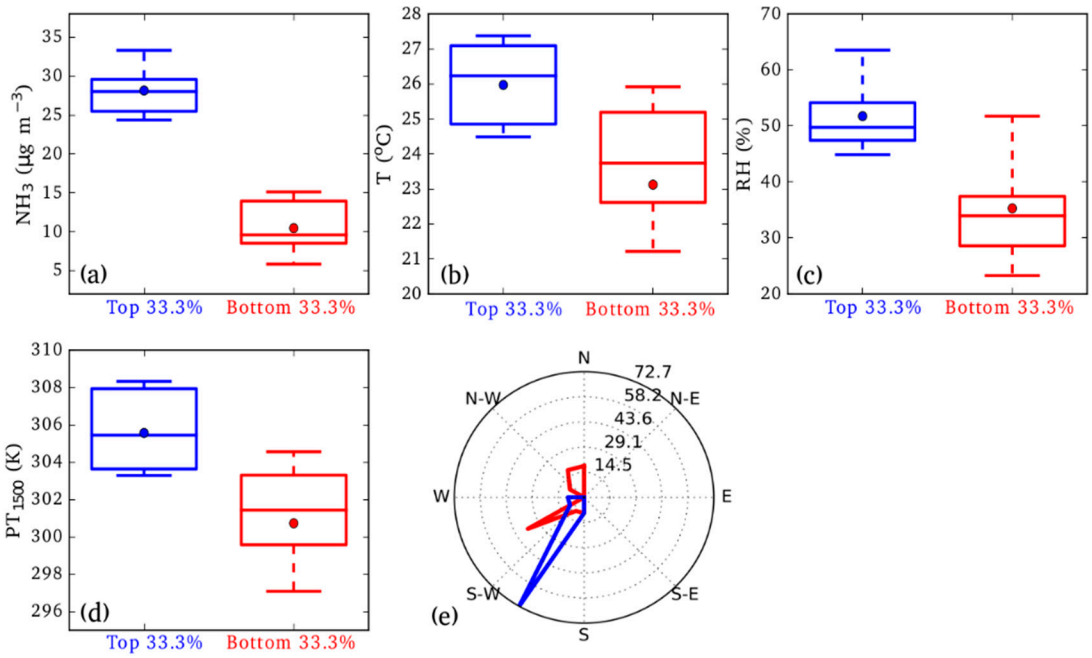

Figure 3. Box-whiskers plots showing different characteristics between the top 33.3% and bottom 33.3% NH_3 concentrations during the dry conditions from 11 May to 24 June, 2015, including (**a**) NH_3

concentrations, (**b**) 2-m T, (**c**) 2-m RH, and (**d**) 1500-m PT. The central box represents the values from the lower to upper quartile (25th to 75th percentile). The vertical line extends from the 10th percentile to the 90th percentile value. The middle solid line represents the median, and the dot represents the mean value. In (**e**), wind rose diagram based on the 800-m horizontal wind associated with the top 33.3% (in blue) and bottom 33.3% (in red) NH_3 concentrations in Beijing are shown. Except for that the 1500-m PT and 800-m wind are shown according to the soundings at 20:00 LT, the other variables are derived from the daily mean values.

3.2. Case Study on the Regional Transport of NH_3 to Beijing using WRF-Chem

In this section, the simulation results were first validated against the observations, and then the impact of regional transport on the NH_3 concentration in Beijing was presented. Figure 4 shows the time series of the observed and simulated NH_3 concentrations, $PM_{2.5}$ concentrations, 2-m Ts, and 2-m RHs in Beijing from 23 to 25 May. Although the model tends to underestimate the daytime NH_3 and $PM_{2.5}$ concentrations in Beijing, both the diurnal pattern (peaking in the early morning and reaching the minimum in the afternoon) and the daily variation were generally well reproduced. The correlation coefficients between the observed and simulated NH_3 and $PM_{2.5}$ concentrations in Beijing were 0.73 and 0.70, respectively (Figure 4a,b). Good agreements also can be found between the observations and simulations of T and RH (Figure 4c,d). In addition to the near-surface parameters, the simulated vertical structures of PT and horizontal wind over Beijing were also compared with the sounding data (Figure 5). The gradual warming of the upper air and the strengthening of southerly winds in Beijing from 23 to 25 May were accurately simulated by the model. Overall, these generally good model performances (Figures 4 and 5) provide a basis to use the simulation results to investigate the transport process during the studied period.

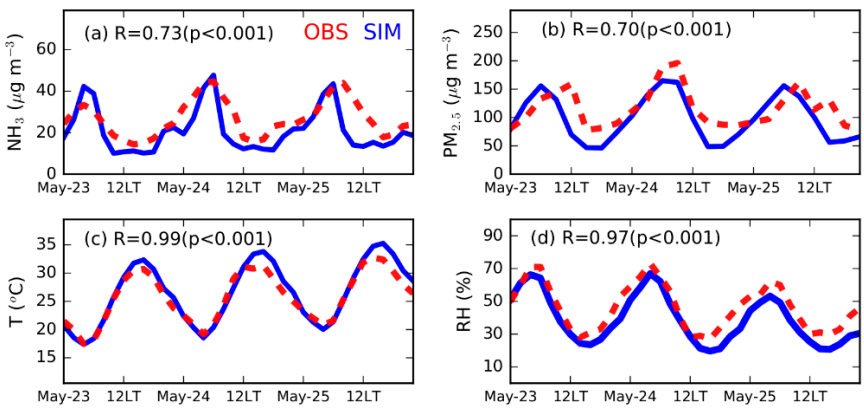

Figure 4. Time series of observed and simulated (**a**) NH_3 concentrations, (**b**) $PM_{2.5}$ concentrations, (**c**) 2-m Ts, and (**d**) 2-m RHs in Beijing from 23 to 25 May, 2015. The correlation coefficients (R) between observations and simulations are presented for each panel.

To identify the possible source regions, 24-h backward trajectories ending at the NH_3 monitoring site in Beijing were simulated using the HYSPLIT. With a high pressure located over the south seas at the 925-hPa level, there was a southeast-to-northwest pressure gradient across Beijing from 23 to 25 May, which supported the southerly prevailing winds towards Beijing (Figure 6). Influenced by such synoptic conditions, the backward trajectories during those three days all passed through the south part of Hebei province. Based on these trajectories and the spatial distribution of NH_3 emissions (Figures 1 and 6), we roughly delimited a potential source region in the southern plains adjacent to Beijing (114.3–118.0° E, 35.8–39.5° N). The EXP simulation was conducted using the emission zero-out configuration in the potential source region. Figure 7 presents the spatial distribution of the ground-level NH_3 concentration in the Beijing–Tianjin–Hebei region at 18:00 LT during the selected episode. The NH_3 concentration in the center of Beijing was around 12 μg m^{-3}, significantly lower than those in the southern upstream plains, in which the NH_3 concentrations were greater than 20 μg m^{-3}

on 24 and 25 May (Figure 7a–c). By calculating the difference between the BASE and EXP runs, the contributions of the potential source region to the NH_3 concentrations in the Beijing–Tianjin–Hebei region were illustrated in Figure 7d–f. At 18:00 LT, the transport process can increase the NH_3 concentration in the center of Beijing by 5–7 μg m^{-3}. Averaging the simulation results of each day, the daily NH_3 concentrations in the center of Beijing were calculated, which were 15.1 μg m^{-3} on 23 May, 15.0 μg m^{-3} on 24 May, and 15.7 μg m^{-3} on 25 May (Figure 8), and the southern plains could contribute 5.4 μg m^{-3} (36%), 6.1 μg m^{-3} (41%), and 5.3 μg m^{-3} (34%), respectively. These results indicate that when the Beijing–Tianjin–Hebei region is influenced by the southerly prevailing winds, the regional transport plays an important role in the NH_3 concentration in Beijing. Thus, joint efforts to reduce NH_3 emissions in the whole Beijing–Tianjin–Hebei region are necessary to regulate the NH_3 concentration in Beijing.

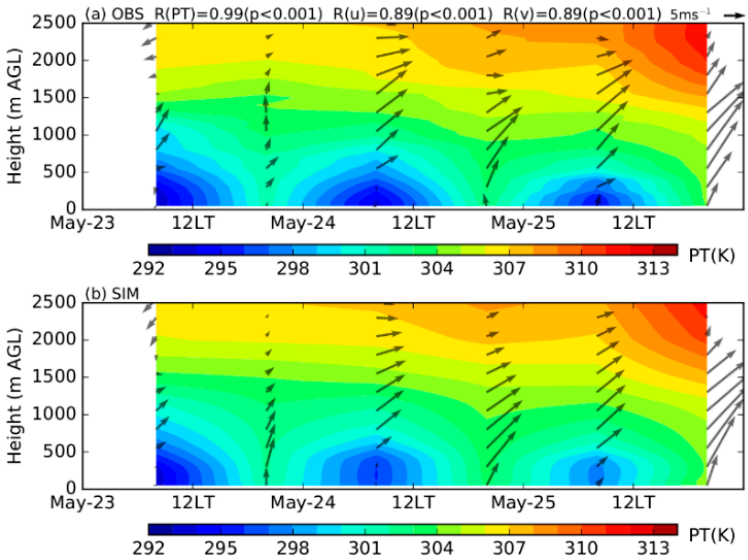

Figure 5. Vertical structures of (**a**) the observed and (**b**) the simulated PTs and horizontal winds in Beijing from 23 to 25 May, 2015. Both simulations and observations are shown with an interval of 12-h. At the top of Figure 5a, the correlation coefficients (R) between simulations and observations are presented.

Besides, to understand the impacts of NH_3 emissions on the $PM_{2.5}$ pollution, we compared the simulated SIA concentrations in the Beijing–Tianjin–Hebei region under different emission scenarios (i.e., BASE, SIM-1 and SIM-2). By halving the emissions of SO_2 and NO_X (Figure 9b), the near-surface SIA concentration in Beijing can decrease by 14.3 μg m^{-3} (41%). Comparing the results of SIM-2 with those of SIM-1, it was found that the control of NH_3 emissions could result in an additional 13% reduction in the SIA concentration in Beijing (Figure 9c). Similar results have also been found by Fu et al. [24]. Thus, enforcing the NH_3 emissions control in conjunction with other gas pollutants can benefit the $PM_{2.5}$ pollution mitigation [2,10,24]. It should be noted that the link between NH_3 and aerosol pollution is quite complicated [23,24,47,48], and here we just presented some results of simplistic numerical experiments, which warrants further studies. To develop the effective emission control policies, the framework that explicitly considers the pH and liquid water content proposed by Nenes et al. [47] can be used to determine the chemical domains of the sensitivity of the aerosol concentration to the NH_3 and HNO_3 levels.

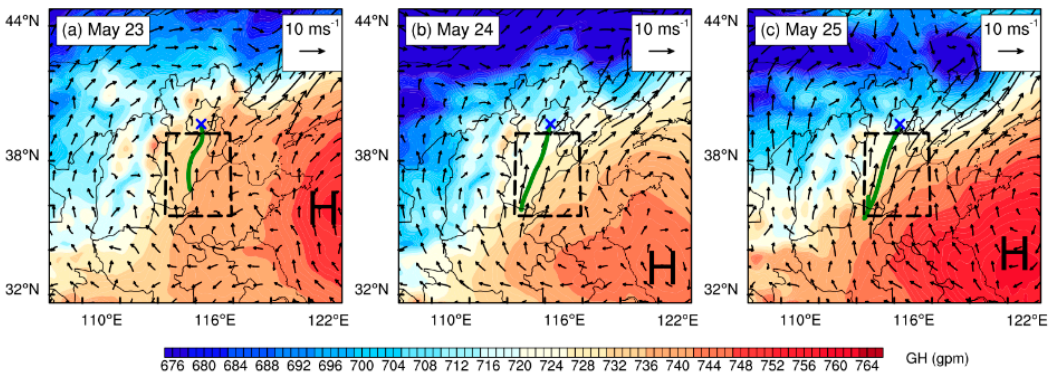

Figure 6. Spatial distributions of 925-hPa geopotential height (GH) and horizontal winds in the simulation domain at 18:00 LT on (**a**) 23 May, (**b**) 24 May, and (**c**) 25 May, 2015, derived from the atmospheric reanalysis of European Centre for Medium-Range Weather Forecasts. The location of the NH_3 monitoring site is marked by the blue cross, and 24-h backward trajectories arriving in the site are shown as the green lines. The dashed rectangle adjacent to Beijing indicates the regions using the emission zero-out method in the WRF-Chem simulation. The high-pressure systems in the southern seas are denoted by the text "H".

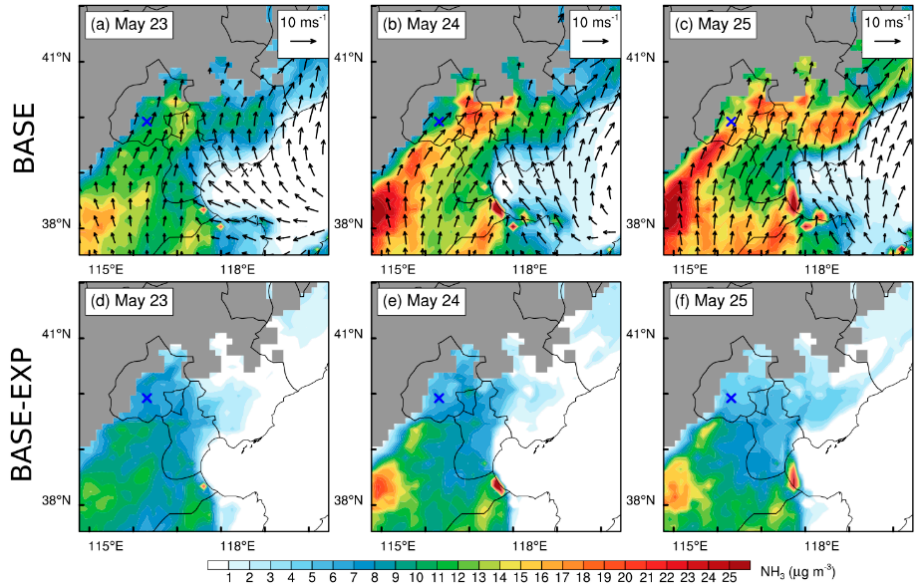

Figure 7. Spatial distribution of the simulated near-surface NH_3 concentrations and winds at 18:00 LT on (**a**,**d**) 23 May, (**b**,**e**) 24 May, and (**c**,**f**) 25 May, 2015. The mountainous regions are denoted by the grey shadings. The top panels show the simulation results of the baseline (BASE) run, and the bottom panels present the differences between the BASE run and sensitivity experiment (EXP). The location of the NH_3 monitoring site in Beijing is indicated by the blue cross.

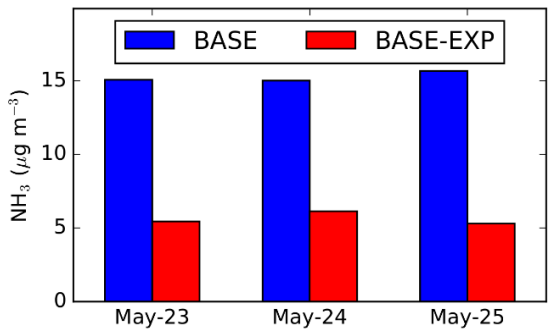

Figure 8. Bar plot showing the daily NH_3 concentrations in Beijing derived from the BASE run and contributed by the southern plain regions (BASE-EXP).

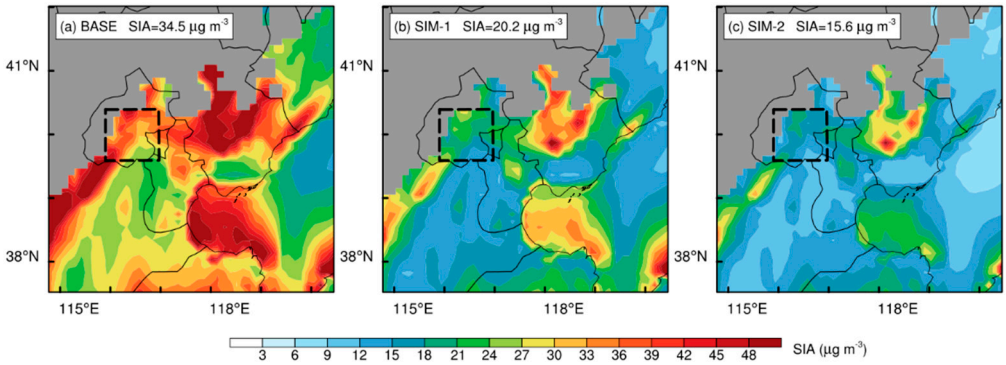

Figure 9. Spatial distributions of near-surface secondary inorganic aerosols (SIA) concentrations in the Beijing–Tianjin–Hebei region during the studied episode derived from the (**a**) BASE run, (**b**) SIM-1 run, and (**c**) SIM-2 run. The average SIA concentrations in the dashed rectangle are given for each panel.

4. Conclusions

In this study, the influence of regional transport on the NH_3 concentration in Beijing was systematically investigated by combining observational analyses, backward trajectory calculations, and meteorology–chemistry coupled simulations. The NH_3 concentration was measured in the Beijing Municipal Environmental Monitoring Center from 11 May to 24 June, 2015.

A statistically significant positive correlation was found between the NH_3 and $PM_{2.5}$ concentrations in Beijing. The relationships between the NH_3 concentrations and meteorological parameters in Beijing were also examined. The daily NH_3 concentration was positively correlated with the near-surface T and RH. The higher NH_3 concentrations in Beijing were usually associated with the warming of the upper atmosphere. The warming aloft can increase the thermal stability, which would suppress the development of the boundary layer to some extent, as well as the vertical dispersion of pollutants. Further, distinct wind directions could be found during the days of the top and bottom 33.3% NH_3 concentrations. The top 33.3% NH_3 concentrations in Beijing were primarily in relation to the southwesterly winds (181–225°), while the bottom 33.3% NH_3 concentrations were corresponding to the westerly and northerly winds (226–360°). Since there are strong NH_3 emissions in the southern plains adjacent to Beijing, the regional transport of NH_3 induced by the southerly prevailing winds plays an important role in the NH_3 concentration in Beijing.

From 23 to 25 May, with a high pressure located over the south seas at the 925-hPa level, there was a southeast-to-northwest pressure gradient across Beijing, which supported the southerly prevailing winds towards Beijing. As a result, the NH_3 emitted from southern Hebei could be easily transported to Beijing, leading to a higher NH_3 concentration in Beijing. Thus, joint efforts to reduce NH_3 emissions in the whole Beijing–Tianjin–Hebei region are necessary to regulate the NH_3 concentration in Beijing. Besides, enforcing the NH_3 emissions control in conjunction with the ongoing stringent control of SO_2 and NO_X emissions can further mitigate the aerosol pollution in Beijing.

Author Contributions: Y.M. and L.W. designed the study, Q.W. and Y.M. conducted the simulations, analyzed, and wrote the manuscript. All authors have read and agreed to the published version of the manuscript.

Funding: This research was funded by from the National Key R&D program of China (2016YFD0201204, 2016YFE0101100, and 2017YFD0201801), National Natural Science Foundation of China (41705002, 21777191).

Acknowledgments: The authors would like to thank China Meteorological Administration for providing meteorological data, China National Environmental Monitoring Center and Beijing Municipal Environmental Monitoring Center for providing air quality measurements, European Centre for Medium-Range Weather Forecasts (ECWMF) for providing the ERA5 reanalysis, and Tsinghua University for providing the emission data. The authors also would like to acknowledge the support from China Scholarship Council (CSC).

Conflicts of Interest: The authors declare no conflict of interest.

References

1. Sutton, M.A.; Reis, S.; Riddick, S.N.; Dragosits, U.; Nemitz, E.; Theobald, M.R.; Tang, Y.S.; Braban, C.F.; Vieno, M.; Dore, A.J.; et al. Towards a climate-dependent paradigm of ammonia emission and deposition. *Philos. Trans. R. Soc. B Biol. Sci.* **2013**, *368*, 20130166. [CrossRef] [PubMed]
2. Behera, S.N.; Sharma, M.; Aneja, V.P.; Balasubramanian, R. Ammonia in the atmosphere: A review on emission sources, atmospheric chemistry and deposition on terrestrial bodies. *Environ. Sci. Pollut. Res.* **2013**, *20*, 8092–8131. [CrossRef] [PubMed]
3. Aneja, V.P.; Roelle, P.A.; Murray, G.C.; Southerland, J.; Erisman, J.W.; Fowler, D.; Asman, W.A.H.; Patni, N. Atmospheric nitrogen compounds II: Emissions, transport, transformation, deposition and assessment. *Atmos. Environ.* **2001**, *35*, 1903–1911. [CrossRef]
4. Chan, C.K.; Yao, X. Air pollution in mega cities in China. *Atmos. Environ.* **2008**, *42*, 1–42. [CrossRef]
5. Miao, Y.; Liu, S.; Guo, J.; Huang, S.; Yan, Y.; Lou, M. Unraveling the relationships between boundary layer height and PM2.5 pollution in China based on four-year radiosonde measurements. *Environ. Pollut.* **2018**, *243*, 1186–1195. [CrossRef] [PubMed]
6. Zhang, X.; Wu, Y.; Liu, X.; Reis, S.; Jin, J.; Dragosits, U.; Van Damme, M.; Clarisse, L.; Whitburn, S.; Coheur, P.-F.; et al. Ammonia Emissions May Be Substantially Underestimated in China. *Environ. Sci. Technol.* **2017**, *51*, 12089–12096. [CrossRef]
7. Lelieveld, J.; Evans, J.S.; Fnais, M.; Giannadaki, D.; Pozzer, A. The contribution of outdoor air pollution sources to premature mortality on a global scale. *Nature* **2015**, *525*, 367–371. [CrossRef]
8. Pozzer, A.; Tsimpidi, A.P.; Karydis, V.A.; de Meij, A.; Lelieveld, J. Impact of agricultural emission reductions on fine-particulate matter and public health. *Atmos. Chem. Phys.* **2017**, *17*, 12813–12826. [CrossRef]
9. Hristov, A.N. Technical note: Contribution of ammonia emitted from livestock to atmospheric fine particulate matter (PM2.5) in the United States. *J. Dairy Sci.* **2011**, *94*, 3130–3136. [CrossRef]
10. Liu, X.; Xu, W.; Duan, L.; Du, E.; Pan, Y.; Lu, X.; Zhang, L.; Wu, Z.; Wang, X.; Zhang, Y.; et al. Atmospheric Nitrogen Emission, Deposition, and Air Quality Impacts in China: An Overview. *Curr. Pollut. Rep.* **2017**, *3*, 65–77. [CrossRef]
11. Pope, C.A., III; Burnett, R.T.; Thurston, G.D.; Thun, M.J.; Calle, E.E.; Krewski, D.; Godleski, J.J. Cardiovascular mortality and long-term exposure to particulate air pollution: Epidemiological evidence of general pathophysiological pathways of disease. *Circulation* **2004**, *109*, 71–77. [CrossRef]
12. Tao, W.K.; Chen, J.P.; Li, Z.; Wang, C.; Zhang, C. Impact of aerosols on convective clouds and precipitation. *Rev. Geophys.* **2012**, *50*, 1–62. [CrossRef]
13. Xu, P.; Zhang, Y.; Gong, W.; Hou, X.; Kroeze, C.; Gao, W.; Luan, S. An inventory of the emission of ammonia from agricultural fertilizer application in China for 2010 and its high-resolution spatial distribution. *Atmos. Environ.* **2015**, *115*, 141–148. [CrossRef]
14. Cheng, Z.; Luo, L.; Wang, S.; Wang, Y.; Sharma, S.; Shimadera, H.; Wang, X.; Bressi, M.; de Miranda, R.M.; Jiang, J.; et al. Status and characteristics of ambient PM2.5 pollution in global megacities. *Environ. Int.* **2016**, *89–90*, 212–221. [CrossRef]
15. Wang, S.; Nan, J.; Shi, C.; Fu, Q.; Gao, S.; Wang, D.; Cui, H.; Saiz-Lopez, A.; Zhou, B. Atmospheric ammonia and its impacts on regional air quality over the megacity of Shanghai, China. *Sci. Rep.* **2015**, *5*, 15842. [CrossRef]
16. Hu, G.; Sun, J.; Zhang, Y.; Shen, X.; Yang, Y. Chemical Composition of PM2.5 Based on Two-Year Measurements at an Urban Site in Beijing. *Aerosol Air Qual. Res.* **2015**, *15*, 1748–1759. [CrossRef]
17. Wei, L.; Duan, J.; Tan, J.; Ma, Y.; He, K.; Wang, S.; Huang, X.; Zhang, Y. Gas-to-particle conversion of atmospheric ammonia and sampling artifacts of ammonium in spring of Beijing. *Sci. China Earth Sci.* **2015**, *58*, 345–355. [CrossRef]
18. Bobbink, R.; Hicks, K.; Galloway, J.; Spranger, T.; Alkemade, R.; Ashmore, M.; Bustamante, M.; Cinderby, S.; Davidson, E.; Dentener, F.; et al. Global assessment of nitrogen deposition effects on terrestrial plant diversity: A synthesis. *Ecol. Appl.* **2010**, *20*, 30–59. [CrossRef] [PubMed]
19. Bowman, A.F.; Van Vuuren, D.P.; Derwent, R.G.; Posch, M. A global analysis of acidification and eutrophication of terrestrial ecosystems. *Water Air Soil Pollut.* **2002**, *141*, 349–382. [CrossRef]
20. Bowman, W.; Cleveland, C.; Halada, Ľ.; Hreško, J.; Baron, J. Negative impact of nitrogen deposition on soil buffering capacity. *Nat. Geosci.* **2008**, *1*, 767–770. [CrossRef]

21. Stevens, C.J.; Duprè, C.; Dorland, E.; Gaudnik, C.; Gowing, D.J.G.; Bleeker, A.; Diekmann, M.; Alard, D.; Bobbink, R.; Fowler, D.; et al. Nitrogen deposition threatens species richness of grasslands across Europe. *Environ. Pollut.* **2010**, *158*, 2940–2945. [CrossRef] [PubMed]
22. Liu, M.; Huang, X.; Song, Y.; Xu, T.; Wang, S.; Wu, Z.; Hu, M.; Zhang, L.; Zhang, Q.; Pan, Y.; et al. Rapid SO2 emission reductions significantly increase tropospheric ammonia concentrations over the North China Plain. *Atmos. Chem. Phys.* **2018**, *18*, 17933–17943. [CrossRef]
23. Lachatre, M.; Fortems-Cheiney, A.; Foret, G.; Siour, G.; Dufour, G.; Clarisse, L.; Clerbaux, C.; Coheur, P.-F.; Van Damme, M.; Beekmann, M. The unintended consequence of SO2 and NO2 regulations over China: Increase of ammonia levels and impact on PM2.5 concentrations. *Atmos. Chem. Phys.* **2019**, *19*, 6701–6716. [CrossRef]
24. Fu, X.; Wang, S.; Xing, J.; Zhang, X.; Wang, T.; Hao, J. Increasing Ammonia Concentrations Reduce the Effectiveness of Particle Pollution Control Achieved via SO2 and NOX Emissions Reduction in East China. *Environ. Sci. Technol. Lett.* **2017**, *4*, 221–227. [CrossRef]
25. Meng, Z.; Xu, X.; Lin, W.; Ge, B.; Xie, Y.; Song, B.; Jia, S.; Zhang, R.; Peng, W.; Wang, Y.; et al. Role of ambient ammonia in particulate ammonium formation at a rural site in the North China Plain. *Atmos. Chem. Phys.* **2018**, *18*, 167–184. [CrossRef]
26. Miao, Y.; Guo, J.; Liu, S.; Liu, H.; Zhang, G.; Yan, Y.; He, J. Relay transport of aerosols to Beijing-Tianjin-Hebei region by multi-scale atmospheric circulations. *Atmos. Environ.* **2017**, *165*, 35–45. [CrossRef]
27. Zhang, Y.; Tang, A.; Wang, D.; Wang, Q.; Benedict, K.; Zhang, L.; Liu, D.; Li, Y.; Collett, J.L.; Sun, Y.; et al. The vertical variability of ammonia in urban Beijing, China. *Atmos. Chem. Phys.* **2018**, *18*, 16385–16398. [CrossRef]
28. Volten, H.; Bergwerff, J.B.; Haaima, M.; Lolkema, D.E.; Berkhout, A.J.C.; van der Hoff, G.R.; Potma, C.J.M.; Wichink Kruit, R.J.; van Pul, W.A.J.; Swart, D.P.J. Two instruments based on differential optical absorption spectroscopy (DOAS) to measure accurate ammonia concentrations in the atmosphere. *Atmos. Meas. Tech.* **2012**, *5*, 413–427. [CrossRef]
29. Chen, F.; Judge, D.; Wu, C.Y.R.; Caldwell, J. Low and room temperature photoabsorption cross sections of NH3 in the UV region. *Planet. Space Sci.* **1998**, *47*, 261–266. [CrossRef]
30. Cheng, G.; Li, J.; Wang, X.; Li, Y.; Zhang, D. Atmospheric ammonia pollution in the traffic environment of Beijing city in spring. *Acta Sci. Circumst.* **2016**, *36*, 2803–2810.
31. Grell, G.A.; Peckham, S.E.; Schmitz, R.; McKeen, S.A.; Frost, G.; Skamarock, W.C.; Eder, B. Fully coupled "online" chemistry within the WRF model. *Atmos. Environ.* **2005**, *39*, 6957–6975. [CrossRef]
32. Chen, F.; Dudhia, J. Coupling an Advanced Land Surface–Hydrology Model with the Penn State–NCAR MM5 Modeling System. Part I: Model Implementation and Sensitivity. *Mon. Weather Rev.* **2001**, *129*, 569–585. [CrossRef]
33. Hong, S.-Y.; Noh, Y.; Dudhia, J. A New Vertical Diffusion Package with an Explicit Treatment of Entrainment Processes. *Mon. Weather Rev.* **2006**, *134*, 2318–2341. [CrossRef]
34. Iacono, M.J.; Delamere, J.S.; Mlawer, E.J.; Shephard, M.W.; Clough, S.A.; Collins, W.D. Radiative forcing by long-lived greenhouse gases: Calculations with the AER radiative transfer models. *J. Geophys. Res.* **2008**, *113*, D13103. [CrossRef]
35. Janjić, Z.I. The Step-Mountain Eta Coordinate Model: Further Developments of the Convection, Viscous Sublayer, and Turbulence Closure Schemes. *Mon. Weather Rev.* **1994**, *122*, 927–945. [CrossRef]
36. Hong, S.-Y.; Dudhia, J.; Chen, S.-H. A Revised Approach to Ice Microphysical Processes for the Bulk Parameterization of Clouds and Precipitation. *Mon. Weather Rev.* **2004**, *132*, 103–120. [CrossRef]
37. Ackermann, I.J.; Hass, H.; Memmesheimer, M.; Ebel, A.; Binkowski, F.S.; Shankar, U. Modal aerosol dynamics model for Europe. *Atmos. Environ.* **1998**, *32*, 2981–2999. [CrossRef]
38. Schell, B.; Ackermann, I.J.; Hass, H.; Binkowski, F.S.; Ebel, A. Modeling the formation of secondary organic aerosol within a comprehensive air quality model system. *J. Geophys. Res. Atmos.* **2001**, *106*, 28275–28293. [CrossRef]
39. Stockwell, W.R.; Middleton, P.; Chang, J.S.; Tang, X. The second generation regional acid deposition model chemical mechanism for regional air quality modeling. *J. Geophys. Res.* **1990**, *95*, 16343–16367. [CrossRef]
40. MEIC Data. Available online: http://www.meicmodel.org (accessed on 21 March 2020).
41. MOZART-4/GEOS-5 Data. Available online: https://www.acom.ucar.edu/wrf-chem/mozart.shtml (accessed on 25 March 2020).

42. Sun, J.; Huang, L.; Liao, H.; Li, J.; Hu, J. Impacts of Regional Transport on Particulate Matter Pollution in China: A Review of Methods and Results. *Curr. Pollut. Rep.* **2017**, *3*, 182–191. [CrossRef]
43. Streets, D.G.; Fu, J.S.; Jang, C.J.; Hao, J.; He, K.; Tang, X.; Zhang, Y.; Wang, Z.; Li, Z.; Zhang, Q.; et al. Air quality during the 2008 Beijing Olympic Games. *Atmos. Environ.* **2007**, *41*, 480–492. [CrossRef]
44. Yoo, J.-M.; Lee, Y.-R.; Kim, D.; Jeong, M.-J.; Stockwell, W.R.; Kundu, P.K.; Oh, S.-M.; Shin, D.-B.; Lee, S.-J. New indices for wet scavenging of air pollutants (O3, CO, NO2, SO2, and PM10) by summertime rain. *Atmos. Environ.* **2014**, *82*, 226–237. [CrossRef]
45. Miao, Y.; Liu, S. Linkages between aerosol pollution and planetary boundary layer structure in China. *Sci. Total Environ.* **2019**, *650*, 288–296. [CrossRef] [PubMed]
46. Miao, Y.; Li, J.; Miao, S.; Che, H.; Wang, Y.; Zhang, X.; Zhu, R.; Liu, S. Interaction between planetary boundary layer and PM2.5 pollution in megacities in China: A Review. *Curr. Pollut. Rep.* **2019**, *5*, 261–271. [CrossRef]
47. Nenes, A.; Pandis, S.N.; Weber, R.J.; Russell, A. Aerosol pH and liquid water content determine when particulate matter is sensitive to ammonia and nitrate availability. *Atmos. Chem. Phys.* **2020**, *20*, 3249–3258. [CrossRef]
48. Guo, H.; Otjes, R.; Schlag, P.; Kiendler-Scharr, A.; Nenes, A.; Weber, R.J. Effectiveness of ammonia reduction on control of fine particle nitrate. *Atmos. Chem. Phys.* **2018**, *18*, 12241–12256. [CrossRef]